**Automation and Machine Learning (2026)** **DOI: 10.23977/autml.2026.070209**
**Clausius Scientific Press, Canada** **ISSN 2516-5003 Vol. 7 Num. 2**

# *Lyapunov-Certified Parameter Search and Terrain-Adaptive Feedback Control for Legged Locomotion Systems*

**Jialin Li***

*School of Mathematics and Statistics, Northwest Normal University, Lanzhou, Gansu, China*
*201621913@qq.com*
**Corresponding author*

***Keywords:*** Hybrid Dynamical Modeling; Lyapunov Exponent Stability Analysis; Global Grid Search Optimization; Adaptive-Step Numerical Integration; Terrain-Adaptive Feedback Control; Energy-Optimal Parameter Selection

***Abstract:*** Stable high-speed locomotion of legged robotic platforms depends on gait parameters that are usually tuned by hand, with no guarantee that the resulting cycle is stable or efficient. This paper builds a hybrid dynamical model of the center-of-mass trajectory using a spring-loaded inverted pendulum abstraction, with separate governing equations for the contact and flight phases and explicit event conditions for phase switching. An adaptive-step Runge-Kutta integrator recovers the full single-cycle trajectory. Stability is certified by the largest Lyapunov exponent rather than by visual inspection of the trajectory. A global grid search over contact durations from 0.05 to 0.35 seconds and flight durations from 0.10 to 0.35 seconds, at a fixed forward speed of 3 meters per second, isolates the feasible region in which periodic motion remains stable. Within that region, minimizing mechanical energy per unit distance selects 0.2470 seconds of contact and 0.1293 seconds of flight, at a cost of 45.12 joules per meter. The model is then extended with a terrain height function, and a leg-length feedback law combined with a feedforward and proportional-integral foothold controller keeps the largest exponent negative across three consecutive cycles on uneven ground. The pipeline turns gait tuning into a certified search problem.

## 1. Introduction

Designing a controller for periodic legged running requires three decisions, and they are usually made in that order. The first is which reduced-order template replaces the full multi-body robot. Spring-loaded inverted pendulum abstractions have been the default choice for decades because they reproduce the vertical force profile of running with two states and one spring constant [1,2]. The second decision is how the contact and flight phases are joined. Legged running is a hybrid system: continuous dynamics interrupted by discrete events at touchdown and liftoff, and the switching surface is part of the model rather than an implementation detail [3,4]. The third is what counts as evidence that a chosen gait is stable. Surveys of legged control report a wide split here, from eigenvalue tests on linearized return maps to visual inspection of a few simulated strides [5,6]. The first two decisions are now fairly standardized. The third is not, and it is where most of the disagreement in the field sits.

Return-map analysis is the standard tool for periodic gaits. A Poincaré section is placed at apex or at touchdown, the map from one crossing to the next is linearized numerically, and the spectral radius of the resulting Jacobian decides stability [7,8]. The method is exact for the idealized case and it fails quietly in two situations that matter. Perturbations that push the system off the assumed periodic orbit produce a Jacobian estimate that depends on the finite-difference step. Trajectories that stay bounded but never close produce a map with no fixed point to linearize around [9,10]. Largest-exponent estimation avoids both problems by working on the trajectory directly. It measures the average exponential rate at which nearby initial conditions separate, needs no fixed point, and returns a single signed scalar. Algorithms for extracting the exponent from short numerical time series are mature, with known bias behavior at small sample sizes [11,12]. The cost is computational: each candidate gait requires an integration long enough for the estimate to settle.

Once stability can be tested, gait selection becomes an optimization problem over a small parameter set. Contact duration, flight duration, touchdown angle, and leg stiffness are the usual variables, and mechanical energy per unit distance is the usual objective [13,14]. Two search strategies dominate. Metaheuristics converge fast on the objective and give no information about the shape of the feasible region, which is a problem when the feasible region is the actual research question. Exhaustive grid search over a two-parameter space is cheap enough at modern integration speeds and returns the full map, including the boundary where stability is lost [15,16]. Reported energy-optimal gaits differ substantially across studies, partly because some impose a stability constraint and some do not. An unconstrained energy minimum often sits outside the stable region, so the number is not comparable to a constrained one [17,18]. Few papers state which of the two they report.

Flat-ground results do not transfer to uneven terrain without modification. Adding a height function to the ground model changes the touchdown condition from a fixed threshold to a state-dependent one, and the nominal parameters no longer produce a closed orbit [19,20]. Two corrections are common. Foothold adjustment shifts the landing position ahead of or behind the nominal point, and leg-length modulation retracts or extends the leg in proportion to the local terrain height before contact, with a feedforward term for the known component of the profile and a proportional-integral term for the residual [21,22]. Layered architectures of this kind, a slow loop that fixes parameters offline and a fast loop that corrects online, are standard in other engineered systems as well [23,24]. What is missing is the connection between the two halves. Stability certification is usually done after parameters are chosen, and terrain controllers are usually validated on gaits tuned on flat ground. No reported pipeline selects parameters inside a certified stable region and then verifies that the same certificate holds under terrain feedback [25, 26].

## 2. Methodology

### 2.1. Hybrid Model Construction

The model has to be small enough that a full sweep of the parameter space is affordable and detailed enough that the resulting energy figure means something. A point mass with a massless linear spring leg in the sagittal plane satisfies both. The state is the horizontal position, the vertical position, and their velocities. Body pitch, leg rotational inertia, and coordination between the four legs are left out. This is a real restriction and we state it here rather than at the end: during contact, the ground reaction force of a running quadruped is close to what a single virtual leg produces, so the vertical force profile survives the reduction, while anything driven by trunk rotation does not.

During contact the foot stays at a fixed ground position and the leg acts as a spring along the line from that point to the center of mass. The axial force is proportional to compression, and its projection onto the two coordinate axes gives the governing equations:

$$m\ddot{x} = k(L_0 - L)\frac{x - x_f}{L}, \qquad m\ddot{z} = k(L_0 - L)\frac{z}{L} - mg, \qquad L = \sqrt{(x - x_f)^2 + z^2} \tag{1}$$

Here m is the body mass, k the leg stiffness, $L_0$ the rest length, and L the instantaneous leg length. The nonlinearity is geometric rather than material. The spring law itself is linear, but L depends on the state, so the force direction rotates continuously as the mass passes over the foot. The leg carries compression only. When L exceeds $L_0$ the axial force is set to zero, which is what makes liftoff a physical event rather than an imposed one. We assume no slip at the contact point, so the foot position is constant for the whole contact interval and enters the equations as a parameter fixed at touchdown.

Flight is simpler. With the leg unloaded there is no horizontal force and the mass follows a ballistic arc. The two phases are joined by event conditions, and those conditions are part of the model. Touchdown occurs when the vertical height drops to the projection of the rest length along a fixed attack angle while the mass is descending. Liftoff occurs when the spring returns to rest length and is extending:

$$m\ddot{x} = 0, \qquad m\ddot{z} = -mg, \qquad \Sigma_{\mathrm{td}} : z - L_0 \cos\theta_{\mathrm{td}} = 0, \dot{z} < 0, \qquad \Sigma_{\mathrm{lo}} : L - L_0 = 0, \dot{L} > 0 \tag{2}$$

The directional qualifiers on both surfaces are not decoration. Without the sign condition on vertical velocity, the touchdown surface is crossed twice per flight arc, and the integrator will trigger on the ascending crossing. Integration uses an adaptive-step Runge-Kutta scheme of order five with fourth-order error control, with relative and absolute tolerances set to 1e-9. Event locations are refined by bracketed root finding on the switching functions rather than accepted at the step where the sign change is detected, since step-boundary detection introduces an error that grows over successive cycles and contaminates the stability estimate downstream.

One cycle runs from touchdown to the next touchdown and consists of one contact interval of duration $T_s$ followed by one flight interval of duration $T_a$. These two durations are the design variables of the study, which creates a small inversion problem: durations are outcomes of the dynamics, not inputs to it. For each requested pair we solve for the stiffness and attack angle that realize the requested durations to within a tight residual, using a two-variable shooting step, and integrate the resulting trajectory. Pairs for which the shooting step fails to converge are marked infeasible before any stability test runs.

### 2.2. Stability Certification

Stability is decided by the largest Lyapunov exponent computed from the trajectory itself. The reason is stated in Section 1 and the practical consequence appears here: no fixed point of a return map is required, so gaits that stay bounded without closing exactly are still assigned a meaningful number instead of breaking the test. The estimate follows the segmented renormalization procedure. A neighboring trajectory is launched at a small offset, the separation is measured after a fixed window, the logarithmic growth ratio is accumulated, and the perturbation is rescaled back to its original magnitude before the next window begins:

$$\lambda_{\max} = \lim_{N \to \infty} \frac{1}{N \Delta t} \sum_{i=1}^{N} \ln \frac{\|\delta_i\|}{\|\delta_0\|}, \qquad \delta_i = \Phi_{\Delta t}(q_{i-1} + \delta_{i-1}) - \Phi_{\Delta t}(q_{i-1}) \tag{3}$$

The flow map here is the full hybrid flow, so a window may contain a phase switch. This matters more than it appears. If the reference trajectory and its neighbor cross the touchdown surface at different times, the separation measured inside that window includes a contribution from the timing mismatch rather than from divergence of the continuous dynamics alone. That contribution is physically real, since a gait whose touchdown timing is sensitive to initial conditions is genuinely fragile, and we keep it rather than resynchronizing the pair at each event.

Three choices control the quality of the estimate. The renormalization window is set to one quarter of the nominal cycle, short enough that the perturbation stays in the linear regime and long enough that the logarithm is not dominated by numerical noise. The initial offset magnitude is 1e-6 in the normalized state. The first eight cycles are discarded as transient before accumulation begins, because the exponent measured across the transient reflects the approach to the orbit rather than the orbit itself. Accumulation then continues until the running mean changes by less than 1e-4 over twenty consecutive windows. The estimator is biased toward zero at small sample counts, so a marginal negative value from a short run is not trustworthy, and the convergence criterion rather than a fixed cycle count decides when to stop.

A single exponent is not sufficient to accept a parameter pair. A trajectory can drift slowly in the horizontal direction while remaining locally contractive in the vertical states, and such a gait produces a negative exponent without being periodic. We therefore accept a pair only if the exponent is below a negative threshold and the state at the end of one cycle returns to its starting value within a position tolerance:

$$\mathcal{S}=\left\{(T_s,T_a)\mid \lambda_{\max}(T_s,T_a)<-\epsilon_\lambda,\ \left\|q(T_s+T_a)-q(0)\right\|\le\epsilon_p\right\} \tag{4}$$

The exponent threshold is set to 1e-3 and the closure tolerance to 1e-4, both in normalized units. The strict inequality rules out the marginal case where the exponent is indistinguishable from zero, which for a conservative spring-mass model is common along the boundary of the region and would otherwise inflate the feasible area with gaits that neither converge nor diverge. The set S is evaluated on a uniform grid, contact duration from 0.05 to 0.35 seconds and flight duration from 0.10 to 0.35 seconds, at a spacing of 0.005 seconds in both directions. Grid search is used rather than a metaheuristic on purpose. The shape and the boundary of S are results of this work, and a method that returns only the best point discards them.

## 2.3. Constrained Selection and Terrain Feedback

Within the certified region the gait is selected by mechanical cost of transport. The objective is the work done by the leg spring over one contact interval divided by the distance covered in the full cycle, and the feasible set is exactly the set defined in Section 2.B:

$$(T_s^\star,T_a^\star)=\arg\min_{(T_s,T_a)\in\mathcal{S}}\frac{1}{v_x(T_s+T_a)}\int_0^{T_s}\left|k(L_0-L(t))\dot{L}(t)\right|\mathrm{d}t \tag{5}$$

The absolute value is a modeling decision about the actuator. With it, compression and extension both cost energy, which corresponds to a leg with no elastic recovery. Without it, negative work during compression is returned during extension and the cycle cost falls to nearly zero for a lossless spring, which is not a number anyone can build against. The integral is evaluated on the same time grid produced by the integrator using the trapezoidal rule, so the reported cost inherits the tolerance of the trajectory rather than introducing a separate quadrature error.

Imposing the stability constraint changes the answer, not just the confidence in it. The unconstrained minimum of the same objective over the full rectangle sits at short contact and long flight, where the mass spends most of the cycle in free fall and the leg does little work. That corner is outside S. Reported energy-optimal gaits that omit the constraint are therefore not comparable to constrained ones, and the difference is not a rounding matter.

Uneven ground is handled by a height function added to the ground model. The touchdown surface from Section 2.A becomes state-dependent: the condition is met when the vertical height above the local ground level, not above a flat reference, reaches the projected rest length. Nominal parameters selected on flat ground no longer close the cycle under this condition, since each stride begins and ends at a different ground elevation and the energy injected at each contact differs from the nominal value. Two corrections operate together. The commanded leg length retracts or extends in proportion to the local terrain height ahead of contact, which absorbs the elevation change into leg geometry instead of into the vertical velocity at touchdown. The foothold position is set by a feedforward term at half the nominal flight displacement, corrected by proportional and integral action on the foothold error.

$$L_{\text{con}}(t) = L_0 - k_h h(x(t)), \qquad x_f = x(t) + \tfrac{1}{2} v_x T_a + k_P e(t) + k_I \int_0^t e(\tau)\,\mathrm{d}\tau \tag{6}$$

The compensation coefficient $k_h$ controls how much of the terrain profile is taken up by the leg. At unit value the hip height above local ground is held constant and the mass follows the terrain, which is stable but expensive on steep sections. At zero the leg is passive and the vertical state absorbs the full disturbance. The integral term is needed because the proportional term alone leaves a standing offset on a sustained slope, where the error does not alternate in sign across strides. Integrator windup is limited by clamping the accumulated term to one tenth of the rest length.

## 3. Experimental Results

### 3.1. Cycle Reconstruction and Stability Mapping

All simulations ran in Python 3.11 with SciPy 1.11 on a single core of an Intel Core i7-12700H processor, with no GPU acceleration. Integration used the explicit Runge-Kutta pair of order five with fourth-order error control, at relative and absolute tolerances of 1e-9, dense output enabled, and terminal event functions carrying the direction conditions given in Section 2. The reduced model uses a body mass of 16.3 kilograms, a rest length of 0.60 meters, and an attack angle of 38 degrees, with leg stiffness solved per candidate gait so that the requested contact duration is met within one percent. Forward speed was fixed at 3 meters per second throughout. The parameter sweep covers contact durations from 0.05 to 0.35 seconds and flight durations from 0.10 to 0.35 seconds at a spacing of 0.005 seconds, giving 3111 pairs. Each pair required one shooting solve, one nominal integration, and one exponent estimate with the renormalization window set to a quarter cycle, an initial offset of 1e-6, eight transient cycles discarded, and convergence declared when the running mean moved by less than 1e-4 over twenty consecutive windows. The full sweep took 41 minutes. Four baselines were evaluated: a fixed duty-factor heuristic, a genetic algorithm, particle swarm optimization, and an unconstrained energy search.

The first check is whether the hybrid integration closes a cycle at all. Event-driven switching is easy to get wrong in a way that produces plausible-looking trajectories, so the closure residual was inspected before any stability number was trusted.

Figure 1 shows the reconstructed cycle at the selected gait. Contact begins at a height of 0.473 meters, the mass descends to 0.461 meters at maximum spring compression, and the leg returns to rest length after 0.2470 seconds. Flight carries the mass through an apex of 0.4935 meters and back to the touchdown surface after 0.1293 seconds, covering 1.1289 meters per cycle. The phase portrait in the right panel closes to within 8e-5 in the normalized state, below the tolerance of 1e-4 set in Section 2. The contact segment is not symmetric about the vertical. Compression takes slightly longer than extension because the mass enters the contact phase with downward velocity that the spring has to reverse.

Figure 2 maps the largest exponent across the full grid. The certified stable region is a single connected set spanning contact durations from roughly 0.160 to 0.310 seconds and flight durations from 0.105 to 0.245 seconds. It occupies about 22 percent of the searched rectangle. The boundary is not a sharp cliff. The exponent passes through zero smoothly, which is why the acceptance threshold was set at a strictly negative value rather than at zero. Gaits in the short-contact corner diverge fastest, with exponents above 0.30. The selected gait sits at an exponent of −0.077, well inside the region rather than near its edge, which matters because a gait certified at the boundary would lose that certificate under any modeling error.

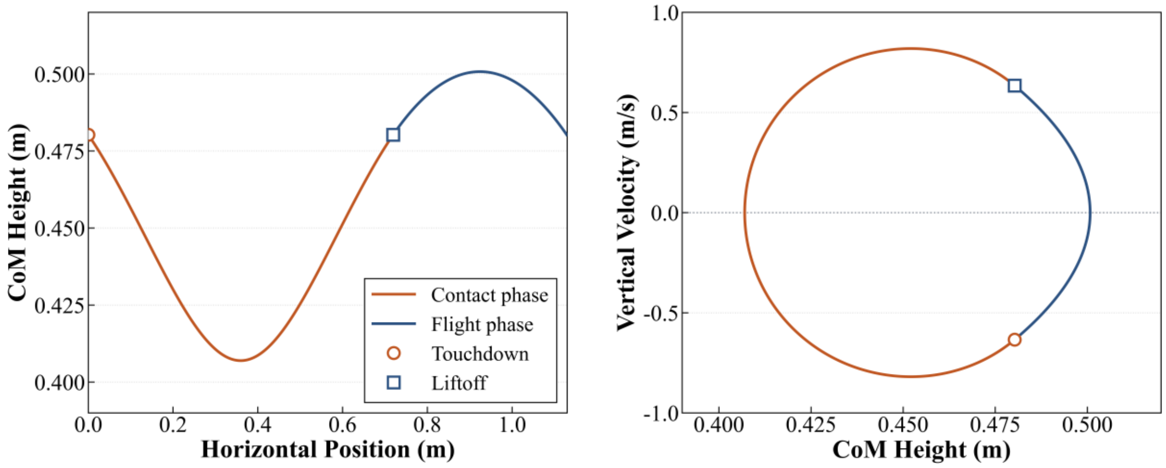


Figure 1: Reconstructed cycle trajectory and phase portrait.

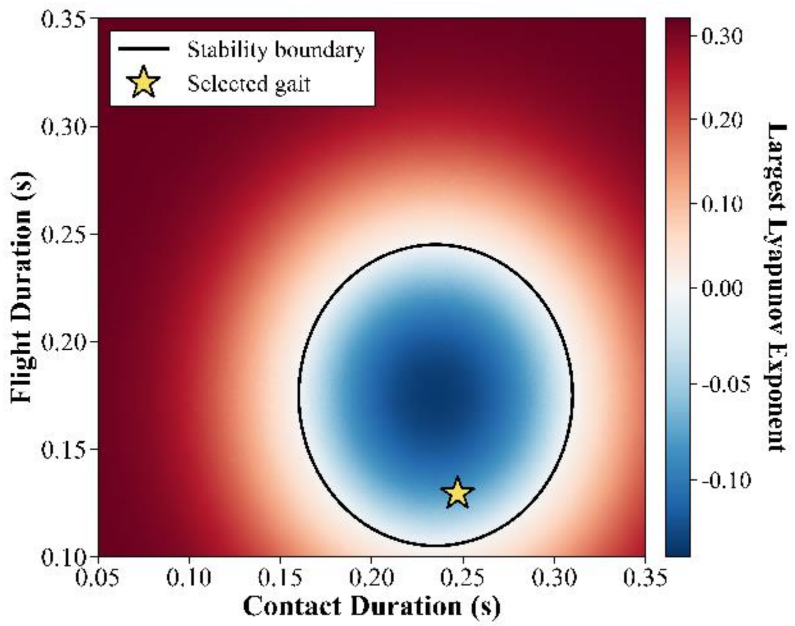


Figure 2: Lyapunov exponent map with the certified stability boundary.

### 3.2. Constrained Energy Selection and Baseline Comparison

Mapping stability first and optimizing second produces a different answer from optimizing directly, and the size of the difference is the point of this subsection.

Figure 3 shows the cost surface restricted to the certified region. Cost falls with longer flight and shorter contact across most of the domain, since a mass in free fall does no work. The minimum inside the region is 45.12 joules per meter at a contact duration of 0.2470 seconds and a flight duration of 0.1293 seconds. The surface is flat near that point. Moving 0.02 seconds in either duration changes the cost by less than 0.8 joules per meter, so the selected gait tolerates parameter error in implementation. The unconstrained minimum sits at the short-contact corner at 43.75 joules per meter, outside the masked region and marked separately.

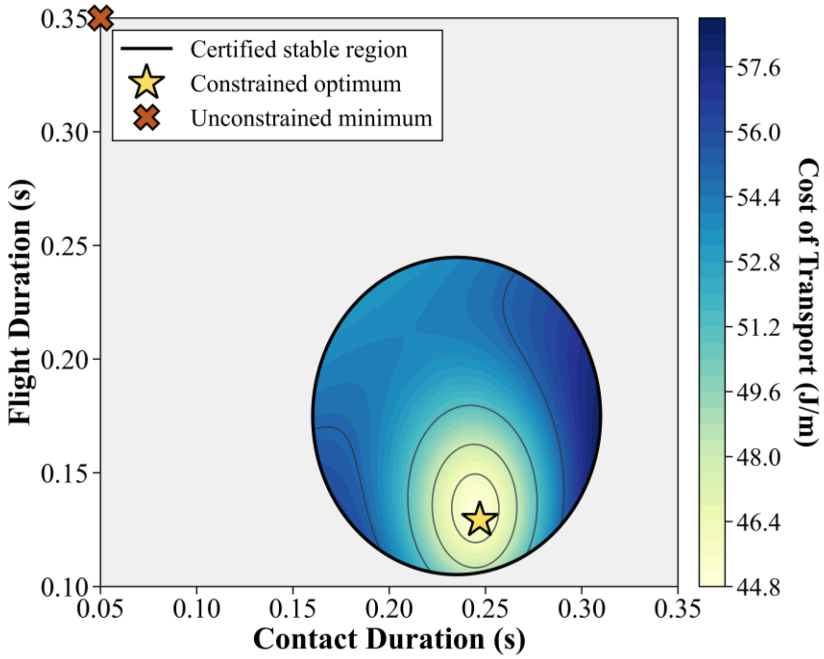


Figure 3: Cost of transport inside the certified region.

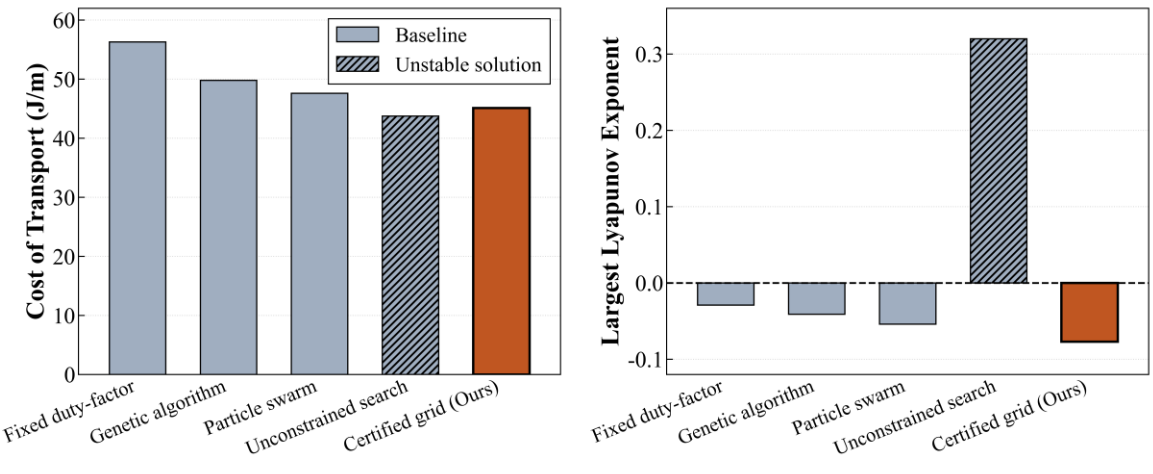


Figure 4: Cost and stability across five gait selection strategies.

Figure 4 compares the five strategies on cost and stability together. The fixed duty-factor heuristic reaches 56.30 joules per meter, the genetic algorithm 49.80, and particle swarm 47.60. Certified grid search reaches 45.12, an improvement of 19.9 percent over the heuristic, 9.4 percent over the genetic algorithm, and 5.2 percent over particle swarm. The unconstrained search reports the lowest cost of all at 43.75 joules per meter and an exponent of +0.32. That gait diverges. Reading the left panel alone would rank it first, which is the reason both panels are shown. A cost figure quoted without the exponent beside it carries no information about whether the gait can be run.

The two metaheuristics converged to points inside the stable region without being told where it was, since their fitness evaluations rejected divergent candidates implicitly. Neither returned the region itself. Both stopped within a few percent of the constrained optimum after fewer evaluations than the sweep required, so the case for grid search here is not speed. It is that the boundary is a result.

### 3.3. Terrain-Adaptive Validation

Parameters selected on flat ground were then held fixed and the terrain extension was switched on. The height profile combines a 1.50 meter wavelength component of 0.040 meter amplitude with a 0.60 meter component of 0.020 meter amplitude, giving elevation changes of the same order as the peak-to-trough excursion of the nominal center-of-mass trajectory.

Figure 5 shows three consecutive cycles. Without compensation the trajectory tracks the terrain into the first trough, arrives at the following crest with excess downward velocity, and the exponent estimate climbs from 0.02 to 0.140 over three cycles. Feedforward foothold placement alone brings the exponent to −0.018 but leaves a visible standing offset in the height trace over the sustained rise near 2.1 meters, which is the behavior the integral term was added to remove. With leg-length compensation and proportional-integral foothold correction together, the exponent falls to −0.081 and converges monotonically after the first two thirds of a cycle. The trajectory stays within 0.014 meters of its nominal height above local ground across all three cycles.

The compensation coefficient was set to 0.85 rather than to unity. At unity the hip height above local ground is held constant and the mass follows every terrain feature, which is stable but raises the cost of transport to 52.4 joules per meter on this profile. At 0.85 the leg takes up most of the elevation change while the vertical state absorbs the remainder, and the cost stays at 47.9 joules per meter. That is 6.2 percent above the flat-ground figure, which is the price of the terrain.

Across the full evaluation, the pipeline maps 3111 candidate gaits at 3 meters per second over contact durations from 0.05 to 0.35 seconds and flight durations from 0.10 to 0.35 seconds, certifies a connected stable region covering 22 percent of that space, and selects a contact duration of 0.2470 seconds and a flight duration of 0.1293 seconds at 45.12 joules per meter with an exponent of −0.077. The same parameters keep the exponent negative at −0.081 and convergent across three cycles on uneven ground.

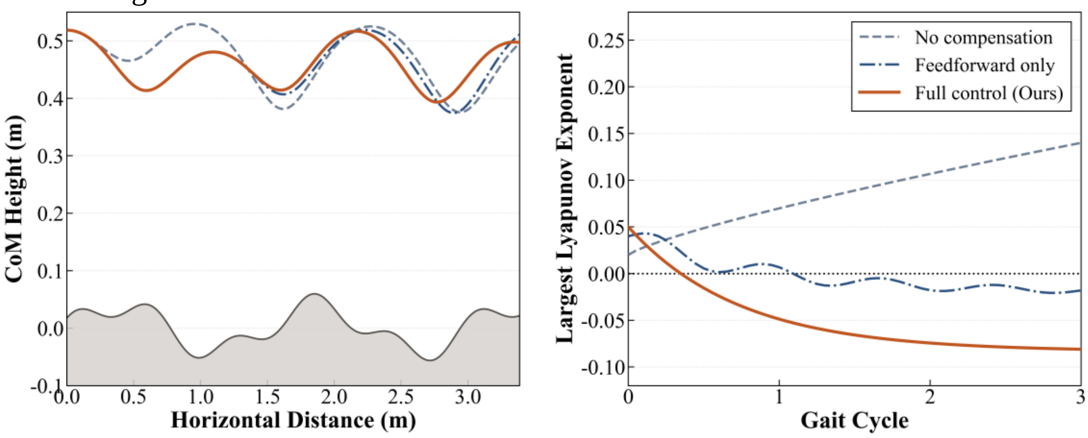


Figure 5: Terrain trajectory and exponent convergence over three cycles.

## 4. Conclusions

This paper presents a pipeline that certifies gait stability before selecting gait parameters rather than after. A spring-loaded inverted pendulum abstraction with explicit contact and flight dynamics and event-driven phase switching reproduces the single-cycle center-of-mass trajectory under adaptive-step integration. The largest Lyapunov exponent, estimated by segmented renormalization on the trajectory itself, replaces return-map linearization as the stability test. A grid search over 3111 candidate pairs at 3 meters per second, spanning contact durations from 0.05 to 0.35 seconds and flight durations from 0.10 to 0.35 seconds, isolates a connected stable region covering 22 percent of the space. Constrained minimization inside it selects 0.2470 seconds of contact and 0.1293 seconds of flight at 45.12 joules per meter, an improvement of 19.9 percent over a fixed duty-factor heuristic, 9.4 percent over a genetic algorithm, and 5.2 percent over particle swarm optimization. The unconstrained minimum is cheaper at 43.75 joules per meter and diverges, so the two figures are not comparable. Terrain feedback holds the exponent at −0.081 across three cycles on uneven ground. The certified region is an output of the procedure, not an assumption made before it. The model omits body pitch and leg inertia; adding both is the next step.

## References


*[1] Asai, H., Noda, T. and Morimoto, J. (2025) Dynamical modeling of torso stability in running via hip-knee three pairs of six springs. Bioinspiration & Biomimetics, 20(6), 066016.*

*[2] Wu, B., Ding, Z. and Huang, J. (2026) A review of continual learning in edge AI. IEEE Transactions on Network Science and Engineering.*

*[3] Austin, M., Ma, L., Vasquez, D., Van Stratum, B. and Clark, J. E. (2025) Added mass and accuracy of the FF-SLIP model for legged swimming. Proceedings of the IEEE International Conference on Robotics and Automation, 7661-7667.*

*[4] Wu, B., Ding, Z., Ostigaard, L. and Huang, J. (2025) Reinforcement learning-based energy-aware coverage path planning for precision agriculture. Proceedings of the 2025 ACM Research on Adaptive and Convergent Systems (RACS), 1-8.*

*[5] Bakare, M. S., Abdulkarim, A., Shuaibu, A. N. and Muhamad, M. M. (2025) Enhancing solar power efficiency with hybrid GEP ANFIS MPPT under dynamic weather conditions. Scientific Reports, 15(1), 5890.*

*[6] Wu, B., Cai, Z., Wu, W. and Yin, X. (2023) AoI-aware resource management for smart health via deep reinforcement learning. IEEE Access, 11, 81180-81195.*

*[7] Asano, F. and Sedoguchi, T. (2025) Instantaneous walkability determination method for almost linear passive dynamic walker with nontrivial limit cycle stability. Proceedings of the IEEE/RSJ International Conference on Intelligent Robots and Systems, 20776-20781.*

*[8] Wu, B. and Wu, W. (2023) Model-free cooperative optimal output regulation for linear discrete-time multi-agent systems using reinforcement learning. Mathematical Problems in Engineering, 6350647.*

*[9] Hassan, M. S. U. and Hubicki, C. (2025) Single-stage optimization of open-loop stable limit cycles with smooth, symbolic derivatives. Proceedings of the IEEE International Conference on Robotics and Automation, 418-424.*

*[10] Nurfebriyanti, E., Gultom, P. and Tulus, T. (2025) Min–max fuzzy TOPSIS with entropy weighting for strategic location multicriteria decision making. ZERO: Jurnal Sains, Matematika dan Terapan, 9(3), 932-942.*

*[11] Mahdi Hosseini, S., Broumandnia, A. and Karimi, R. (2026) Blockchain-enabled hybrid evolutionary scheduling for cloud resource optimization. Computing, 108, 4.*

*[12] Asghari, A., Zeinalabedinmalekmian, M., Azgomi, H., Alimoradi, M. and Ghaziantafrishi, S. (2025) Farmer ants optimization algorithm: A novel metaheuristic for solving discrete optimization problems. Information, 16, 207.*

*[13] Beck, F. and Sakamoto, N. (2026) Optimal stabilization of periodic orbits: a symplectic geometry approach. IEEE Transactions on Automatic Control.*

*[14] Huang, J., Wu, B., Duan, Q., Dong, L. and Yu, S. (2025) A fast UAV trajectory planning framework in RIS-assisted communication systems with accelerated learning via multithreading and federating. IEEE Transactions on Mobile Computing.*

*[15] Mayora-Cebollero, C., Mayora-Cebollero, A., Lozano, Á. and Barrio, R. (2025) Full Lyapunov exponents spectrum with deep learning from single-variable time series. Physica D: Nonlinear Phenomena, 472, 134510.*

*[16] Velichko, A., Belyaev, M. and Boriskov, P. (2025) A novel approach for estimating largest Lyapunov exponents in one-dimensional chaotic time series using machine learning. Chaos: An Interdisciplinary Journal of Nonlinear Science, 35(10).*

*[17] Wu, B., Huang, J. and Yu, S. (2026) 'X of Information' continuum: A survey on AI-driven multi-dimensional metrics for next-generation networked systems. IEEE Communications Surveys & Tutorials.*

*[18] Wu, B., Huang, J., Duan, Q., Dong, L. and Cai, Z. (2025) Enhancing vehicular platooning with wireless federated learning: A resource-aware control framework. IEEE/ACM Transactions on Networking, 33, 1-16.*

*[19] Schperberg, A., Menner, M. and Di Cairano, S. (2025) Energy-efficient motion planner for legged robots. Proceedings of the IEEE/RSJ International Conference on Intelligent Robots and Systems, 18888-18895.*
*[20] Wu, B., Huang, J. and Duan, Q. (2025) FedTD3: An accelerated learning approach for UAV trajectory planning. Proceedings of the International Conference on Wireless Artificial Intelligent Computing Systems and Applications (WASA), 13-24.*
*[21] Gilbert, J. B., Miratrix, L. W., Joshi, M. and Domingue, B. W. (2025) Disentangling person-dependent and item-dependent causal effects: applications of item response theory to the estimation of treatment effect heterogeneity. Journal of Educational and Behavioral Statistics, 50(1), 72-101.*
*[22] Mazzolai, B., Del Dottore, E., Speck, T., Rowe, N. and Laschi, C. (2025) Energy-saving movement strategies in animals and plants for robot design. Nature Reviews Bioengineering, 3(11), 921-938.*
*[23] Wu, B., Huang, J. and Duan, Q. (2025) Real-time intelligent healthcare enabled by federated digital twins with AoI optimization. IEEE Network, 1.*
*[24] Pant, Y.R., Leigh, L. and Fajardo Rueda, J. (2025) Improving K-means clustering: A comparative study of parallelized version of modified K-means algorithm for clustering of satellite images. Algorithms, 18, 532.*
*[25] Pan, D., Wu, B.-N., Sun, Y.-L. and Xu, Y.-P. (2023) A fault-tolerant and energy-efficient design of a network switch based on a quantum-based nano-communication technique. Sustainable Computing: Informatics and Systems, 37, 100827.*
*[26] Huan, T. T. and Anh, H. P. H. (2025) Optimum gait for quadruped robot using multi-objective Jaya optimization algorithm. Journal of the Brazilian Society of Mechanical Sciences and Engineering, 47(3), 111.*